Reflectivity, Ice Scattering, and Lightning Characteristics of Hurricane Eyewalls and Rainbands. Part I: Quantitative Description

DANIEL J. CECIL*

Department of Atmospheric Sciences, Texas A&M University, College Station, Texas

EDWARD J. ZIPSER AND STEPHEN W. NESBITT

Department of Meteorology, University of Utah, Salt Lake City, Utah

(Manuscript received 3 January 2001, in final form 17 August 2001)

ABSTRACT

Covering December 1997 through December 1998, 261 overpasses of 45 hurricanes by the Tropical Rainfall Measuring Mission (TRMM) satellite are used to document the observed radar reflectivity values, passive microwave ice scattering magnitudes, and total lightning (cloud to ground plus in cloud). These parameters are interpreted as describing convective vigor or intensity, with greater reflectivities (particularly aloft), greater ice scattering (lower 85- and 37-GHz brightness temperatures), and increased lightning frequency indicating more intense convection. For each parameter, the full distribution of values observed during the TRMM satellite's first year is presented for specific regions. Properties of three regions of the hurricane (eyewall, inner rainband, and outer rainband) are treated separately and compared to other tropical oceanic and tropical continental precipitation systems. Reflectivity profiles and ice scattering signatures are found to be fairly similar for both hurricane and nonhurricane tropical oceanic precipitation systems, although the hurricane inner rainband region yields the weakest of these convective signatures. When normalized by the area experiencing significant convection, the outer rainband region produces more lightning than the rest of the hurricane or nonhurricane tropical oceanic systems. As a whole, the tropical oceanic precipitation systems (both hurricane and nonhurricane) are dominated by stratiform rain and relatively weak convection.

1. Introduction

Convective systems over the tropical oceans produce weaker vertical motions than their continental counterparts (LeMone and Zipser 1980; Jorgensen and LeMone 1989; Lucas et al. 1994; Igau et al. 1999). Despite extreme horizontal wind speeds, the vertical motions encountered in tropical cyclones are typically rather modest (Jorgensen et al. 1985; Black et al. 1996), with magnitudes similar to those found in ordinary tropical oceanic convection. These vertical motions are normally too weak to suspend large ice particles or supercooled raindrops above the melting level (Black and Hallett 1986, 1999). The resulting ice layer microphysics are consistent with observations of 1) sharp decreases in radar reflectivity above the melting level (Jorgensen et al. 1985; Szoke et al. 1986; Black et al. 1996), 2) modest passive microwave ice scattering signatures (Cecil and Zipser 1999), and 3) weak electric fields (Black and Hallett 1986, 1999) and low lightning flash rates (e.g., Ligda 1955; Black et al. 1986; Samsury and Orville 1994; Lyons and Keen 1994; Molinari et al. 1999). This study will quantify the range and frequency of observations of radar reflectivity profiles, passive microwave ice scattering signatures, and lightning occurrence in distinct regions of the tropical cyclone. The properties associated with these regions will be compared with each other and with properties from a large sample of tropical oceanic and tropical continental precipitation systems.

The motivation for subdividing the tropical cyclone into three separate regions comes from the observation that tropical cyclone outer rainbands tend to produce more lightning than either eyewalls or inner rainbands (e.g., Molinari et al. 1999). Inner rainbands (those in the region immediately outward from the eyewall) produce the least lightning and also produce slightly weaker vertical motion and vertical reflectivity profiles than eyewalls. Otherwise, eyewalls and inner rainbands have been found to be somewhat comparable to other tropical oceanic convective systems (e.g., Jorgensen et al. 1985;

* Current affiliation: National Space Science and Technology Center, University of Alabama in Huntsville, Huntsville, Alabama.

Corresponding author address: Daniel J. Cecil, National Space Science and Technology Center, University of Alabama in Huntsville, 320 Sparkman Dr., Huntsville, AL 35805.
E-mail: Daniel.Cecil@msfc.nasa.gov

Szoke et al. 1986; Black et al. 1996). This would seem to imply that either 1) the outer rainbands occupy the most vigorous end of the spectrum of tropical oceanic convection, 2) the eyewalls and inner rainbands have lower lightning flash rates despite being comparable in other regards to general tropical oceanic convection, or 3) the outer rainbands have higher lightning flash rates despite being comparable in other regards to general tropical oceanic convection. If statement 1 above is true, *lower* passive microwave brightness temperatures (''strong'' ice scattering signatures) and *higher* radar reflectivity values aloft should occur preferentially in the outer rainbands. This would suggest that parameterizations and retrieval algorithms that are suitable for the normally weak convection often found over the tropical oceans are not as well suited to the more intense convection found in hurricane outer rainbands. If statement 2 or 3 is true, all of these categories would have fairly similar distributions of brightness temperatures and reflectivity profiles, but dissimilar lightning flash rates. This would suggest that lightning observations contain independent information about some subtle yet important microphysical distinction between the regimes being studied.

Besides comparing these individual regions of the hurricane, it is important to document the frequency of occurrence of particular radar reflectivity or ice scattering magnitudes. As cloud resolving models generate hydrometeor fields with realistic spatial patterns, it is often difficult to assess the accuracy of the *magnitudes* of these fields. Radar reflectivity or passive microwave brightness temperatures can often be derived from the output hydrometeor fields. The large sample of radar and passive microwave observations in this study provides guidelines against which such model output can be checked. Understanding the observations of reflectivity and brightness temperature is also fundamental if we are to assess rainfall retrievals based on these observations and the application of such retrievals to climate studies (Rodgers et al. 2000) or forecasting (Tibbets and Krishnamurti 2000). The purpose of this study is to *quantify and understand differences* in the remotely sensed properties of eyewalls, inner rainbands, and outer rainbands, and also to *document the range of observed values* of radar reflectivity and ice scattering signature in these features.

2. Organization of precipitation in hurricanes

Since the earliest radar observations of tropical cyclones, a distinction has been noted between the somewhat uniform, quasi-circular rainbands near the cyclone center and the more cellular, spiral-shaped bands farther from the center (e.g., Wexler 1947; Ligda 1955; Senn and Hiser 1959). More recently, Willoughby et al. (1984) identified the stationary band complex (SBC), a common feature found at the boundary of the vortex core and the environmental envelope. The Rossby number is of order unity in this location, which places the SBC near the center of weak hurricanes and farther away in strong hurricanes. The SBC has three components, although all three are not always present: the principal band, the connecting band, and the secondary bands. The SBC may coexist with the eyewall or with concentric eyewalls.

The categorizations used in this study are motivated by the three distinct regions Molinari et al. (1999) identified using radial profiles of lightning flash counts. These categories are 1) the eyewall region, 2) the inner rainband region, and 3) the outer rainband region. An example of these is given in Fig. 1a. The guidelines used here are strongly guided by Willoughby et al. (1984) description of the SBC.

The *eyewall region* is a quasi-circular ring of precipitation surrounding the circulation center. It is not required that an eyewall be completely closed, as many mature hurricanes have incomplete eyewalls. The eyewall merely must be identifiable in the radar and/or passive microwave data used in this study. In the case of concentric eyewalls, both eyewalls are included in the eyewall region. Willoughby (1990) and Samsury and Zipser (1995) noted that while the dynamics of the outer and inner eyewall are essentially the same, the outer eyewall may be somewhat weak and short lived or it may contain vigorous convection and cause the inner eyewall to dissipate as the outer eyewall contracts.

The *inner rainband region* typically extends from the eyewall outward about 100 km. It is usually bounded on the outside by a precipitation free lane adjacent to a prominent outer rainband, and often connects the downwind tip of this outer rainband to the eyewall.

The *outer rainband region* typically begins at 150–200-km radius from the cyclone center and includes any rain features associated with the cyclone and located beyond this distance. The innermost outer rainband often is a prominent spiral-shaped feature whose downwind tip merges with the eyewall or with the mass of inner rainband precipitation surrounding the eyewall.

The description of the inner rainband region is similar to the description of secondary and connecting bands by Willoughby et al. (1984), while the feature marking the outer rainband region is similar to the principal band described by Willoughby et al. In many cases, the principal band *does* mark the innermost outer rainband. In other cases (particularly when the SBC is located near the cyclone center), the principal band is included with the inner rainbands. In these cases, a longer rainband generally matching the principal band's description is usually found at a greater distance from the center. This study is not limited to banded features; more uniform areas of precipitation fill many gaps between rainbands.

In most cases, the eyewall slopes significantly outward with height. As a result, the upper-level portion of the eyewall extends above stratiform rain adjacent to the low-level eyewall. Ideally, this stratiform rain would be included with the inner rainband region while the

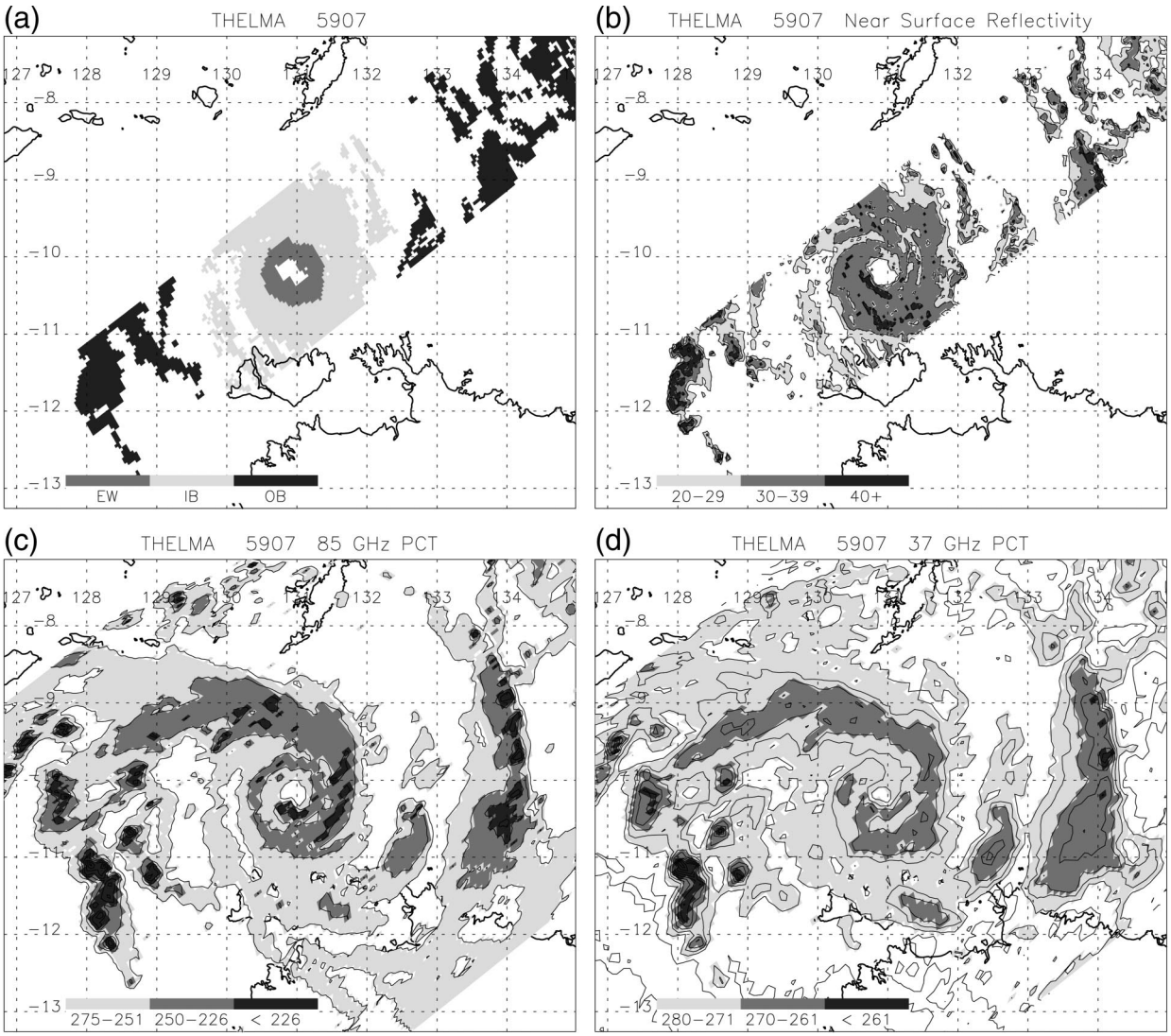

FIG. 1. Examples of (a) eyewall region, inner rainband region, and outer rainband region classifications; (b) PR near-surface reflectivity (dBZ); (c) TMI 85-GHz PCT (K); and (d) TMI 37-GHz PCT (K) from Cyclone Thelma, TRMM orbit 5907, at 1053 UTC 7 Dec 1998. Several lightning flashes (not shown) are associated with the outer rainband near 128° longitude.

upper-level portion of the eyewall would be included with the eyewall region. In practice, part of the stratiform rain is included with the eyewall region in some cases and part of the upper-level eyewall is included with the inner rainband region in some cases. This limitation is due to both the spatial resolution of the data and the necessity of applying a single boundary between regions at all vertical levels.

Jorgensen et al. (1985) examined the vertical motion characteristics encountered during radial aircraft penetrations of four intense, mature Atlantic hurricanes. That only intense hurricanes (with central pressures ranging from 91.2 to 95.5 kPa) were selected may bias the data relative to this study, particularly for the eyewall region, which is more closely related to hurricane intensity than the rainband regions. Each penetration was subjectively divided into an eyewall region and rainband region, with the cutoff generally occurring about 10 km beyond the radius of maximum wind. The cutoff was chosen such that the convection of the outermost eyewall was included in the eyewall region, but any adjacent stratiform rain would be included in the rainband region. This cutoff is similar to the philosophy used in this study, although comparatively coarse resolution may require that part of the adjoining stratiform rain be included with the eyewall region. Jorgensen et al.'s penetrations typically extended about 130 km from the cyclone center, but were sometimes extended to include strong rainbands within about 160 km of the center. Therefore, Jorgensen et al.'s rainband sample likely includes some observations that would be considered outer rainbands. However, the majority of the rainband sample conforms

to the inner rainband definition used in this study. This is demonstrated by Fig. 2 of Jorgensen (1984), showing radar imagery from the four hurricanes investigated by Jorgensen et al. They found updraft sizes and magnitudes to be lognormally distributed. At the 90th percentile, eyewall updrafts had slightly greater peak magnitudes (8 m s^{-1}) than the nonhurricane convective cells (7 m s^{-1}) in the Global Atmospheric Research Program (GARP) Atlantic Tropical Experiment (GATE) studied by LeMone and Zipser (1980). Rainband updrafts had a slightly weaker magnutide (6 m s^{-1}). All of these *peak* updraft magnitudes are less than even the *mean* updraft magnitudes from continental regions (>10 m s^{-1}). Subsequent studies from other tropical oceanic regions (Jorgensen and LeMone 1989; Lucas et al. 1994; Igau et al. 1999) agree that updraft magnitudes over tropical oceans are similar for both hurricane and nonhurricane convection, with hurricane eyewalls producing slightly stronger updrafts. Implications for this study are that indicators of convective vigor (i.e., reflectivity profiles, ice scattering signatures, and lightning) should be somewhat similar for both hurricane and nonhurricane tropical oceanic systems, with the eyewall region yielding more intense convective signatures than the inner rainband region.

Szoke et al. (1986) examined radar reflectivity profiles obtained in two of the hurricanes studied by Jorgensen et al. (1985), in addition to several GATE convective systems and the flight from which Barnes et al. (1983) studied a hurricane inner rainband. Szoke et al. classified precipitation cells as eyewall, rainband, or bright band. As in Jorgensen et al., the rainband category is likely similar to the inner rainband category used in the current study. Complicating matters, ''bright band'' (stratiform) is not one of the fundamental categories in the current study, although for some purposes data will be separated into stratiform and convective components. Szoke et al. determined the maximum reflectivity as a function of height for individual cells and presented mean profiles of this maximum reflectivity. The mean eyewall reflectivity profile had greater reflectivity aloft and a smaller decrease of reflectivity with height than either the rainband profile or the GATE profile. However, continental reflectivity profiles from the literature had *much* greater reflectivity aloft. These results can be compared qualitatively to those presented in section 6, but differences in methodology and radar properties (e.g., minimum detectable signal, beamwidth, calibration) limit any quantitative comparisons.

Black et al. (1996) examined vertical incidence Doppler radar data (reflectivity and velocity) obtained in seven Atlantic hurricanes. Central pressures during the research flights ranged from 89.2 to 97.0 kPa, with most in the 95–96-kPa range. Again, there may be a bias toward intense, mature hurricanes. Radial flight legs were subjectively divided into eyewall, rainband, stratiform, and ''other'' regions. Eyewall regions were defined by quasi-circular reflectivity maxima in the horizontal and elongated reflectivity maxima in the vertical. Rainbands included those regions outside the eyewall having local reflectivity maxima exceeding 30 dB*Z* and having greater vertical extent than the surrounding area. Stratiform regions consisted of horizontally homogeneous reflectivity patterns with values of 10–30 dB*Z* and usually included a brightband feature. The remaining (''other'') features were typically adjacent to eyewalls or rainbands, but had reduced reflectivity values and lower radar echo tops. In the current study, the horizontal reflectivity and 85-GHz ice scattering fields are used to subjectively define the eyewall, inner rainband, and outer rainband regions. The Black et al. criteria involving the vertical extent of high reflectivity in the eyewalls and rainbands are more restrictive, as is the 30-dB*Z* reflectivity requirement in the rainband region. The intention is to isolate convective features. The current study can make direct comparisons to these only after isolating stratiform and convective components. The radial legs in the Black et al. dataset typically extend about 100 km from the hurricane center, so the stratiform and rainband regions generally correspond to the inner rainband region in this study. Black et al. retrieved vertical velocities and analyzed these in a manner similar to Jorgensen et al. (1985). The results were quite similar to Jorgensen et al., but the Black et al. dataset extends these results through the vertical (as opposed to the distinct flight levels analyzed by Jorgensen et al.). The difference in updraft magnitudes between eyewalls and inner rainbands is apparently greater at higher altitudes. Reflectivity differences between these regions correspondingly increase with height and significant radar echoes extend to greater heights in the eyewalls. As with Szoke et al. (1986), the reflectivity profiles presented by Black et al. can only be compared qualitatively with the reflectivity profiles of this study.

Molinari et al. (1999) examined the spatial and temporal distribution of cloud-to-ground lightning flashes in nine Atlantic hurricanes and in the prehurricane stages of three of these storms. These hurricanes were less intense than some of those in the Jorgensen et al. (1985), Szoke et al. (1986), and Black et al. (1996) studies and were all located near the United States. Instead of identifying specific eyewall or rainband regions, the flashes were grouped based on their radial distance from the cyclone center (up to 300 km). A local maximum in flash density was found at a distance of 20–80 km from the center. A minimum extended about 100 km beyond this region, with the greatest flash rate density located 200–300 km from the center. These regions correspond to those occupied by the eyewall, inner rainbands, and outer rainbands in the current study. The flash rate density and the ratio of positive to negative flashes as a function of radius was used to diagnose the inner rainband region as being predominantly stratiform. In comparing Molinari et al.'s results to the lightning observed in this study, it is important to note that this study deals with both cloud-to-ground and intracloud lightning, the

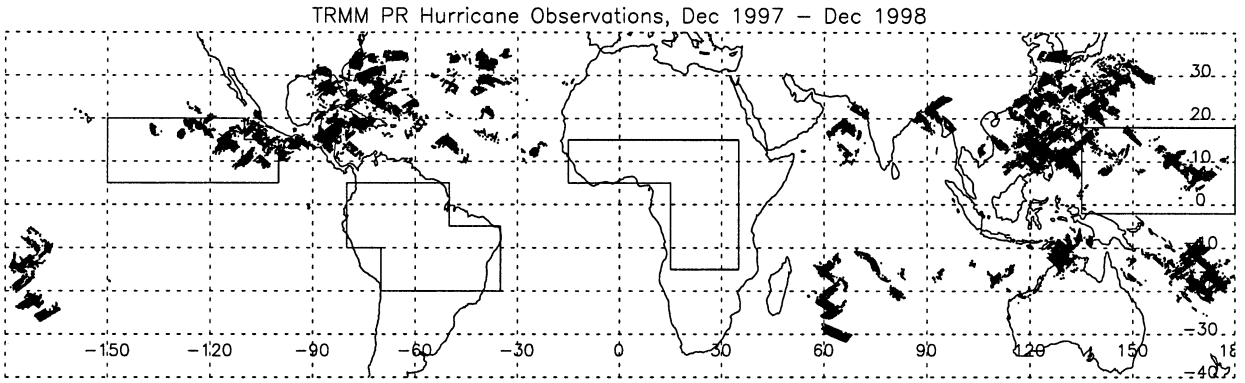

FIG. 2. Geographic distribution of hurricane observations in the database. Nesbitt et al. (2000) tropical continental and tropical oceanic region outlines are included.

minimum detectable flash rate is limited to about one flash per minute, and Molinari et al.'s cases are near or over land at relatively high latitude.

The categorizations used in this study are made *subjectively*, based on the horizontal fields of reflectivity and 85-GHz ice scattering and following the guidelines outlined above. The distinction between eyewall and inner rainband region is made at the outer edge of the horizontal gradient of reflectivity or ice scattering, although the width of the eyewall is limited to about 30 km. In some cases, the gradient of ice scattering would give an inappropriately wide eyewall; the outer boundary of the eyewall is somewhat arbitrary in these cases. (These cases also pose a problem for scattering-based rainfall retrieval algorithms, as the scattering signature extends *beyond* the heavy rain associated with it.) When there is doubt about where to make the distinction between inner rainband and outer rainband, the 150–200-km radius for an increase in lightning flash density found by Molinari et al. (1999) is taken into consideration. There is no predefined limit on the distance of an outer rainband from the cyclone center. Any precipitation features that can be readily identified as part of the hurricane's circulation are included. The categories outlined above are applied to hurricanes in which an eyewall can be identified, or to tropical storms in which an eyewall can be identified and it is expected that the storm is at or near hurricane intensity. In practice, these guidelines yield a maximum eyewall radius ~175 km, minimum inner rainband radius ~30 km, maximum inner rainband radius ~350 km, minimum outer rainband radius ~100 km, and maximum outer rainband radius ~1000 km for the dataset used here. Some of these distances may seem unreasonably large, but were attained in Supertyphoon Zeb near Taiwan. The median radii for the eyewall region, inner rainband region, and outer rainband region are 50, 135, and 350 km, respectively.

3. Data

The data types involved in this study include simultaneous observations of brightness temperature from the Tropical Rainfall Measuring Mission (TRMM) Microwave Imager (TMI), three-dimensional reflectivity from the TRMM Precipitation Radar (PR), and lightning flashes from the Lightning Imaging Sensor (LIS). These instruments are carried on the TRMM satellite. TMI and PR are described in Kummerow et al. (1998, 2000) and Iguchi et al. (2000); LIS is described in Christian et al. (1999).

Data for this study have been collected for all tropical cyclones observed by the TRMM satellite beginning 8 December 1997 (when the PR began data collection) and ending 31 December 1998. The results presented here (restricted to the PR swath) represent the 45 hurricanes or tropical storms with distinguishable eyewalls that were seen by the PR. The geographic distribution of the 261 satellite overpasses is given in Fig. 2. TRMM data collected by Nesbitt et al. (2000) for two tropical oceanic and two tropical continental regions are included in this study for comparison. For analysis and discussion of these nonhurricane precipitation features, the reader is referred to Nesbitt et al. (2000) and Toracinta et al. (2002).

a. Data sources

1) PR

The PR is a 13.8-GHz radar with a 17° scan angle about nadir, resulting in a 215-km-wide swath. Resolution is 4.3 km (horizontal) and 250 m (vertical) at nadir; away from nadir, the horizontal resolution increases at the expense of the vertical resolution. Reflectivities above about 17 dBZ can be detected reliably. Standard algorithms developed for the TRMM program produce attenuation-corrected reflectivity, near-surface reflectivity, rainfall rate, and rain-type (stratiform or convective) products, which are used in this study. [Details on these algorithms can be found online at http://tsdis.gsfc.nasa.gov and are available from the TRMM Science Data and Information System (TSDIS) at NASA Goddard Space Flight Center (GSFC), Greenbelt, Maryland.] Emphasis in this study is placed on reflectivities

above the freezing level, where attenuation correction is rarely an issue. Products from TRMM version 4 processing are used; subsequent reprocessing should have little effect on the results of this study, as the use of derived products (rain type, rainfall rate) is limited.

2) TMI

The TMI is a passive microwave radiometer viewing earth's surface with a 49° nadir angle. Of interest to this study are the 85- and 37-GHz channels. Their effective fields of view are 7 km × 5 km and 16 km × 9 km, respectively, with each scan 760 km wide. The distance between scans is 14 km, so the 85-GHz channel is subject to undersampling and all other frequencies are subject to oversampling.

3) LIS

The LIS retrieves lightning by recording optical pulses in the near-infrared. Both in-cloud and cloud-to-ground flashes are recorded; no distinction is made between these. LIS has an approximately 600 km × 600 km field of view. Any point in this field of view is observed for about 80 s. Horizontal resolution is on the order of 5 km. Of importance to the current study are the *relative* probabilities of lightning for different categories of precipitation features. Therefore, the details of the flash algorithms are somewhat unimportant (assuming the algorithms are equally effective in each regime studied). The 80-s view time limits what can be said about low flash rate storms. This view time limit combined with a *preliminary* estimate of detection efficiency of 75% yields an effective minimum flash rate of approximately 1 flash per minute (Boccippio et al. 2000). This is actually a rather vigorous flash rate for tropical oceanic/hurricane convection, where a few flashes *per hour* are more common. However, a large sample of short duration observations can provide meaningful information, with the understanding that lower flash rate storms are misidentified as being free of lightning.

b. Interpretation of TRMM observations

1) RADAR REFLECTIVITY

Radar reflectivity depends on hydrometeor phase and the sixth power of hydrometeor diameter (Battan 1973) for Rayleigh scattering. This sixth-power dependence is valid for drops that are small compared to the radar wavelength. For the PR (2.2-cm wavelength), drops smaller than about 3 mm behave this way. The largest raindrops, graupel, and hail are in the Mie scattering regime. In this case, a particle's scattering coefficient generally increases, but with a damped oscillation about the diameter squared (geometric area). Because of the nonlinear dependence on diameter, reflectivity responds preferentially to the largest hydrometeors in a sample volume. Liquid water has a greater dielectric constant than ice, so liquid drops are responsible for a reflectivity 7 dBZ greater than ice particles the same size. Above the freezing level, high reflectivity values are indicative of supercooled liquid raindrops or large ice hydrometeors produced by substantial convective updrafts. The rate of decrease of reflectivity above the freezing level can be a rough proxy for updraft speed and consequently supercooled cloud liquid water content (Jorgensen et al. 1985; Zipser and Lutz 1994; Black et al. 1996; Black and Hallett 1999). The relationship between updraft speed and supercooled liquid water is especially rough, as the availability of cloud condensation nuclei (or freezing nuclei and natural seeding) exerts a control on the production (or depletion) of liquid water. Condensation nuclei are especially plentiful in continental air masses, while freezing nuclei and freezing surfaces are abundant in eyewall and inner rainband regions (where frozen hydrometeors spiral into downstream updrafts and act as seeding agents). In the absence of strong updrafts, reflectivity (along with liquid water content) decreases rapidly with height above the freezing level.

2) PASSIVE MICROWAVE ICE SCATTERING

Passive microwave brightness temperatures at both 85 and 37 GHz respond to scattering of upwelling radiation by precipitation-sized ice, which reduces the observed brightness temperature (Wu and Weinman 1984; Wilheit 1986; Spencer 1986; Spencer et al. 1989). This result is termed an ice scattering signature. The magnitude of this ice scattering signature depends on the optical depth, which in turn depends on such factors as the wavelength, the vertical distribution of hydrometeors, and the phase, density, size, and concentration of these hydrometeors. Because of its shorter wavelength, 85 GHz (3.5-mm wavelength) is more sensitive to smaller ice particles than is 37 GHz (8.1-mm wavelength). Particles with diameters several hundred microns or larger are in the Mie regime at 85 GHz, but only O(mm) size particles are in the Mie regime at 37 GHz. Emission by water also contributes to the brightness temperature (TB), but the scattering properties will be focused on in this study. Effects of the underlying surface can be minimized by combining the vertically and horizontally polarized channels, yielding a polarization corrected temperature (PCT). At 85 GHz, Spencer et al. (1989) developed the relationship

$$\mathrm{PCT}_{85} = 1.82\ \mathrm{TB}_{85\mathrm{V}} - 0.82\ \mathrm{TB}_{85\mathrm{H}}, \qquad (1)$$

where the V and H in the subscripts represent vertical and horizontal polarization, respectively.Using a similar empirical approach, we develop the following relation for 37 GHz:

$$\mathrm{PCT}_{37} = 2.20\ \mathrm{TB}_{37\mathrm{V}} - 1.20\ \mathrm{TB}_{37\mathrm{H}}. \qquad (2)$$

The magnitude of 85-GHz scattering, as indicated by

the PCT, has been used to characterize the vigor and spatial extent of convective systems (e.g., Mohr and Zipser 1996; Mohr et al. 1999; Cecil and Zipser 1999; Nesbitt et al. 2000). PCT and the horizontally and vertically polarized brightness temperatures all tend toward equal values as scattering increases (as brightness temperature decreases). At higher brightness temperatures but in the absence of surface effects, we find that PCT can be roughly converted to horizontally or vertically polarized brightness temperatures by the following empirical relations:

$$TB_{85H} \cong -25 + 1.05PCT_{85} \quad (3)$$

$$TB_{85V} \cong -11 + 1.02PCT_{85} \quad (4)$$

$$TB_{37H} \cong -28 + 1.08PCT_{37} \quad (5)$$

$$TB_{37V} \cong -1 + 0.99PCT_{37}. \quad (6)$$

The terms brightness temperature and PCT will be used interchangeably, with the understanding that PCT values are being presented and analyzed in this study.

3) LIGHTNING

Various experiments identify collisions between small cloud ice and larger graupel (growing at the expense of supercooled cloud water) as being responsible for noninductive charge separation leading to lightning (Reynolds et al. 1957; Takahashi 1978; Jayaratne et al. 1983; Illingworth 1985; Saunders et al. 1991; Saunders and Peck 1998). Based on observations from aircraft penetrations of hurricane inner cores, Black and Hallett (1986, 1999) note that updrafts sufficiently strong to produce significant supercooled water and large graupel (and therefore significant charge separation) are somewhat rare in hurricanes. Supercooled water is further limited due to erosion by the plentiful amounts of ice found in hurricanes. Black and Hallett (1999) suggest that the preferred location for those rare instances of significant electrification is the interface between a strong eyewall updraft and adjacent downdraft. They stress the importance of redistribution of ice by the horizontal wind, which can be strongly sheared in both the vertical and horizontal directions.

These three observables (radar reflectivity, passive microwave ice scattering, and lightning) react in different ways to the microphysical makeup of a precipitation system. However, they are not wholly independent of each other. Each provides some independent information but must be consistent with the others. Together they paint a picture of the intensity (or lack thereof) and coverage of convection in a precipitation system.

4. Methods

For each tropical cyclone satellite overpass, the regions described in section 2 are subjectively identified based on the 85-GHz and/or reflectivity patterns. Inside these regions, precipitation features are identified based on criteria developed for this study and for a companion study of tropical continental and tropical oceanic convection by Nesbitt et al. (2000). These criteria require at least four contiguous pixels on the PR grid having at least 20 dBZ near surface reflectivity *or* 85-GHz PCT of 250 K or less. The minimum size for one of these features (one with only four pixels) is 75 km^2. The precipitation feature dataset studied by Nesbitt et al., consisting of August, September, and October 1998 observations from the tropical western Pacific, tropical eastern Pacific, tropical Africa, and tropical South America, is used here for comparison with the hurricanes of this study. Mohr et al. (1999) note that tropical South American convection during the wet season shares characteristics with tropical oceanic convection instead of purely tropical continental convection. However, this study utilizes data from the transition season, during which the convection there does seem more characteristic of an interior tropical continent (Petersen and Rutledge 2001). Petersen and Rutledge warn against overgeneralizing tropical oceanic convection, noting increased variability in the convective structures within about 1000 km of coasts. The oceanic samples in this study do merge the ''isolated oceanic'' and ''coastal/oceanic'' classifications of Petersen and Rutledge, but only in the deep Tropics, where the isolated/coastal oceanic distinction does not appear to be as important as elsewhere. Although Nesbitt et al. and Toracinta et al. (2002) note some differences between the western and eastern Pacific and between Africa and South America, these are treated here as representing general tropical oceanic precipitation systems and general tropical continental precipitation systems.

Two basic approaches are taken to quantify the properties of precipitation features in this study. In the first approach, the distribution of observations from all data points in all precipitation features is considered. This approach addresses the spatial and temporal frequency of occurrence of any reflectivity value or ice scattering signature in a population of precipitation features. It must be stressed that *the observations are from within precipitation features, and are not inclusive of the nonraining areas in the hurricane environment.* In the second approach, each precipitation feature is assigned a single value for some parameter of interest (size, minimum 85-GHz PCT, minimum 37-GHz PCT, maximum reflectivity at each height interval, lightning flash count) in order to assess that precipitation feature's size or convective intensity. This approach addresses the likelihood that an individual precipitation feature has a certain size or intensity. Because of the limited observational swath (215 km), the size and intensity distributions from the second approach are necessarily biased low. A precipitation feature may extend beyond the edge of the swath, in which case the observed size or convective intensity is merely a lower limit on the feature's

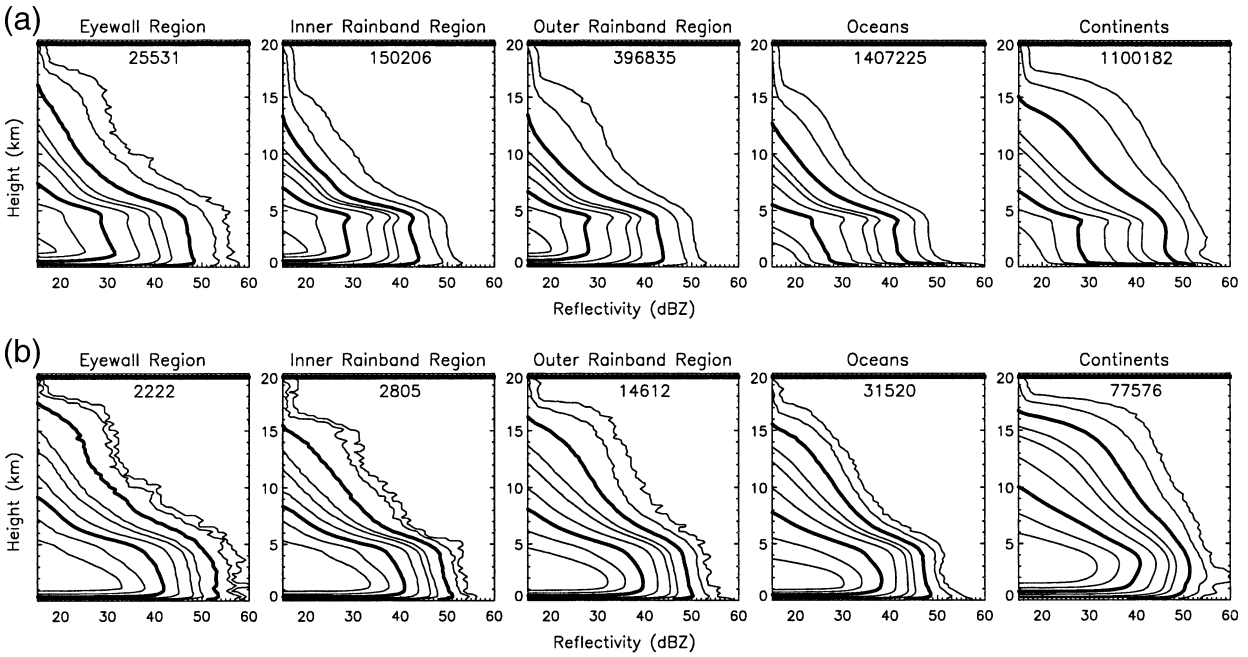

FIG. 3. Cumulative density function of radar reflectivity (1-dBZ intervals) as a function of height. Contour levels are 10%, 25%, 50% (bold), 75%, 90%, 95%, 99% (bold), 99.9%, and 99.99%. Sample size is listed for each region. (a) All data points in precipitation features. (b) Convective certain (TRMM version 4 rain type 20; see section 5a) data points only.

true size or convective intensity. This restriction is not an issue in the first approach.

5. Observed characteristics of precipitation

a. Radar reflectivity characteristics

The database as a whole is dominated by stratiform rain and weak convection, as indicated by enhanced reflectivity values near the freezing level (the radar bright band) and sharp decreases in reflectivity just above the freezing level (Fig. 3a). Table 1 lists the percentages of data points classified as either ''stratiform certain'' or ''convective certain'' (rain types 10 and 20, the most restrictive classifications, from the version 4 TRMM PR algorithm 2A23) for each category of precipitation feature. In most cases, there is ambiguity in either the vertical or horizontal reflectivity structure and neither of these rain types is assigned. The point of this analysis is not to document the actual ratio of stratiform to convective precipitation, but instead to point out that obviously stratiform precipitation is found most readily in the rainband regions and that obviously convective precipitation is found most readily in the eyewall region. The inner rainband region and the general tropical oceanic category are least likely to exhibit a clear convective signal (only 2% of the data pixels in these categories). In the cumulative distribution of reflectivity in Fig. 3a, even the 99th percentile of reflectivity for both the inner rainband region and the general tropical oceanic sample has a brightbandlike maximum near the freezing level. The disparity between the eyewall region and the inner rainband region owes partly to the definitions of each region. The inner rainband region begins on the outside (stratiform) edge of the horizontal gradients that bound the eyewall.

For any of the categories except the general tropical oceanic sample, around half of the area covered by precipitation features has a radar echo below the PR minimum detectable signal ($\approx$17 dBZ) immediately above the freezing level (Table 2, second column). In the tropical oceanic sample, this is true for two-thirds of the area. Only 5% of the rainband and tropical oceanic samples have measurable radar echo extending above about 9-km altitude. At 3-km altitude (in the liquid rain, but above any surface contamination), the median reflectivity is around 28 dBZ for all of the categories except the

TABLE 1. Percentages of data points classified as stratiform certain (TRMM version 4 rain type 10) and convective certain (rain type 20) by the PR. Regions are eyewall (EW), inner rainband (IB), and outer rainband (OB).

	EW region	IB region	OB region	Oceanic	Continental
Total pixels	25 531	150 206	396 835	1 407 225	1 100 182
Stratiform	24.9%	43.7%	41.7%	23.9%	29.0%
Convective	8.7%	1.9%	3.7%	2.2%	7.1%

TABLE 2. Median, 75th, 95th, and 99th percentiles of reflectivity at 3-, 6-, and 9-km altitude.

	50th percentile			75th percentile			95th percentile			99th percentile		
	3 km	6 km	9 km	3 km	6 km	9 km	3 km	6 km	9 km	3 km	6 km	9 km
EW region	29	19	—	35	23	—	42	30	21	47	37	26
IB region	28	18	—	33	22	—	38	26	18	42	29	21
OB region	27	17	—	32	21	—	38	26	18	43	32	22
Oceanic	24	—	—	30	19	—	37	24	17	41	30	21
Continental	28	17	—	33	22	—	41	31	22	46	39	31

general tropical oceanic sample, for which the median is 24 dBZ.

Because stratiform rain dominates the distribution of reflectivity in Fig. 3a, the reflectivity profiles identified as ''convective certain'' are isolated in Fig. 3b. As expected, the decrease of reflectivity with height above the freezing level is much less when considering only the convection. This decrease is noticeably greater for the inner rainband region than for any of the other categories, indicating that the convection in this region tends to be rather weak. The decrease for the tropical continental sample is much less than that for any of the hurricane or other tropical oceanic samples. Even when restricted to those points identified with certainty as convection according to the PR, the median PR echo-top height is only around 8 km in the rainbands and the general tropical oceanic sample. In the eyewall region, the median height of the PR echo top is about 9 km. This altitude difference could be explained by the warm thermal anomaly associated with the eye. Assuming a moist-adiabatic lapse rate, this would correspond to about 6-K warming in the eyewall. This is consistent with observations of the increase in radar brightband height in some radar cross sections spanning the eyewall and adjacent inner rainband region.

To compare the more intense convection from each sample, the 95th percentile of reflectivity for the convective certain points is plotted in Fig. 4. As a first-order approximation, all of the hurricane and other tropical oceanic samples have similar reflectivities through the mixed phase and ice layers, and these reflectivities are much less than those found in the tropical continental regions. At low levels (in the rain layer), reflectivities range from about 45 dBZ for the tropical oceanic sample to nearly 50 dBZ in the eyewall region. For both of the rainband regions, low-level reflectivities are 46–47 dBZ. The inner rainband region's rapid decrease of reflectivity with height causes it to have the lowest reflectivity values throughout most of the mixed phase and ice layers. The eyewall region has slightly greater reflectivities aloft than the outer rainband region, which has slightly greater reflectivities aloft than the general tropical oceanic sample. Again, the enhanced eyewall reflectivities aloft could be due in part to the temperature anomaly. At lower altitudes, the enhanced eyewall reflectivities may result from larger drop sizes; Marks et al. (1993) noted eyewall reflectivities up to 5 dBZ greater than rainband reflectivities associated with the same rain rates. Unlike the extremes of the inner rainband region and the tropical continental sample, the remaining samples have fairly similar slopes of reflectivity with height, suggesting roughly similar convective intensities.

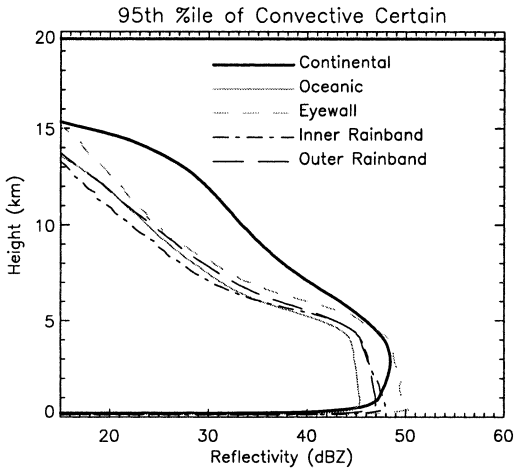

FIG. 4. The 95th percentile of reflectivity for convective certain (TRMM version 4 rain type 20; see section 5a) data points.

The abundance of low reflectivity values, local reflectivity maxima near the freezing level, and sharp decreases of reflectivity just above the freezing level are consistent with the reflectivity distributions presented by Black et al. (1996). The Black et al. mean reflectivity profiles have much greater reflectivity aloft for eyewalls than for rainbands, which is similar to the results presented above, assuming Black et al.'s rainbands are comparable to the convective portions of the inner rainband region in this study. The local reflectivity minimum near 1.5-km altitude noted by Marks and Houze (1987) and Black et al. is not apparent in this dataset. However, PR reflectivities appear most trustworthy at higher altitudes, where attenuation issues and possible contamination from the surface are not an issue.

b. Ice scattering characteristics

Just as the distributions of radar reflectivity are dominated by stratiform rain with low reflectivity above the freezing level, the distributions of 85- and 37-GHz PCT (Figs. 5 and 6, and Table 3) are dominated by very weak or nonexistent ice scattering (high PCT values). In the

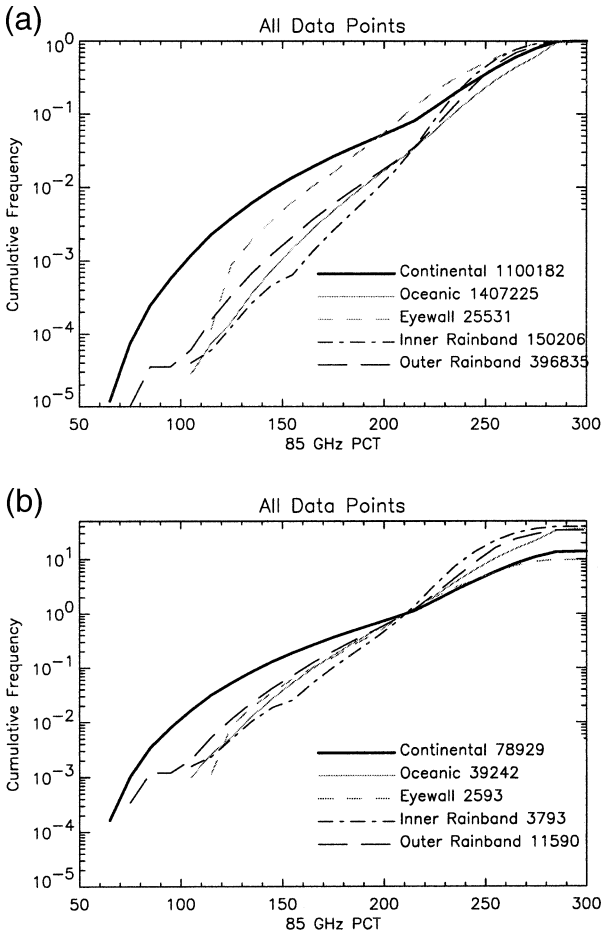

FIG. 5. Cumulative density function of 85-GHz PCT (10-K intervals) for all data points in precipitation features. Sample size (on the PR grid) is listed for each region. (a) All data points in precipitation features. (b) Normalized by the number of points with 85-GHz PCT ≤ 215 K, with the number of points ≤215 K listed.

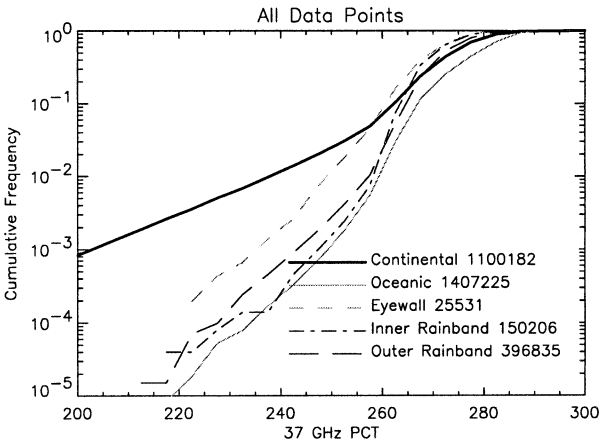

FIG. 6. Cumulative density function of 37-GHz PCT (5-K intervals) for all data points in precipitation features. Sample size (on the PR grid) is listed for each region.

tropical oceanic sample, 81% of the observations have 85-GHz PCTs greater than 250 K. This threshold is exceeded by 72% of the outer rainband region, 63% of the inner rainband region, and 55% of the eyewall region (Table 3). Mohr and Zipser (1996) used a 250-K 85-GHz PCT threshold as a proxy for moderate rainfall in defining mesoscale convective systems. Although 250 K at 85 GHz usually corresponds to a greater rain rate ($\approx$3 mm h^{-1}) than 20-dBZ reflectivity ($\approx$0.5 mm h^{-1}), it is surprising and noteworthy that so much of the area experiencing rainfall (at least 20-dBZ radar reflectivity) has an 85-GHz PCT above this value.

In order to focus on the strong ice scattering that does occur, the cumulative distribution of 85-GHz PCTs is normalized by the number of data points with 85-GHz PCTs of 215 K or less (Fig. 5b). This allows an ''apples to apples'' comparison of the scattering accomplished in the eyewall region to the scattering accomplished in other regions, eliminating the bias from high brightness temperatures. This 215-K brightness temperature threshold was chosen because the percentage of TMI data points meeting this threshold in each sample closely matches the percentage of PR data points classified as convective certain *and* this value represents significant ice scattering at 85 GHz. There is a spatial correspondence between this brightness temperature and the PR-derived convective certain classification, but also some independence. At best this brightness temperature can only identify *deep* convection with a well-developed ice layer. Some of the cumulative distributions in Fig. 5a kink near this brightness temperature; this is most evident in the distribution of tropical continental 85-GHz PCT. This kink, with an increased frequency of PCT values just above 215 K, may represent a distinction between stratiform and convective rain.

With the above normalization (and a similar normalization for 37 GHz) applied, the tropical continental ice scattering signatures are much greater (lower PCT) than those from the other samples, again reflecting the tremendous difference in convective intensities between land and ocean. This difference is most evident at 37 GHz (not shown), which requires larger ice (more vigorous updrafts) to scatter the upwelling radiation. At very low 85-GHz PCTs, the outer rainband region approaches the curve for the tropical continental sample. This represents a tiny portion of the dataset in which outer rainbands are located over land and have char-

TABLE 3. Cumulative frequencies (%) of 85-GHz PCT and 37-GHz PCT below selected thresholds.

	85-GHz PCT			37-GHz PCT		
	≤150 K	≤200 K	≤250 K	≤250 K	≤260 K	≤270 K
EW region	0.40	4.4	44.7	0.93	5.8	45.4
IB region	0.05	0.9	37.1	0.11	1.0	40.2
OB region	0.14	1.5	27.7	0.21	1.3	29.2
Oceanic	0.08	1.4	19.0	0.09	0.7	14.0
Continental	0.97	4.7	30.2	2.19	5.4	27.4

TABLE 4. Lightning flash counts for each region and ratios of various aspects of sample size to flash count.

	Flash count	Precipitation area (km^2) per flash	Near-surface rain per flash (10^6 m^3 h^{-1})	Convective certain area (km^2) per flash	85 GHz $\leq$ 215 K area (km^2) per flash	37 GHz $\leq$ 263 K area (km^2) per flash
EW region	21	22 500	171	2100	2300	2800
IB region	37	75 100	301	1400	1900	3200
OB region	387	19 000	70	700	600	700
Oceanic	329	79 100	243	1800	2200	1600
Continental	36 022	600	3	40	40	60

acteristics of tropical continental convection. Care has been taken to make sure that such cases do not unduly impact any results *discussed* in this paper. In comparison to the tropical continental sample, the hurricane and tropical oceanic samples are tightly clustered over much of the parameter space. Upon closer inspection of those parts of the plots with 85-GHz PCT $\leq$ 200 K (and 37-GHz PCT $\leq$ 260 K, not shown), the inner rainband region produces strong ice scattering least often. Whereas the cumulative distributions normalized by the total number of points in the precipitation feature database (Figs. 5a, 6) suggests that strong ice scattering occurs preferentially in the eyewall region, the normalization used in Fig. 5b and similarly for 37 GHz removes this apparent preference. With this normalization, the ice scattering achieved in the eyewall region is extremely similar to that achieved in the outer rainband region, and is only slightly greater than that achieved in the general tropical oceanic sample. The discrepancy between Figs. 5a and 5b arises because high PCT values with little or no ice scattering make up a much larger proportion of the rainband and general tropical oceanic samples than of the eyewall region sample.

The brightness temperature ranges discussed above compose a small fraction of the total dataset (similar to the convective fractions in Table 1). Histograms of brightness temperatures (not shown) indicate that high brightness temperatures ($\geq$275 K at 85 GHz, with little or no ice scattering) are most frequent in the tropical oceanic sample, followed by the tropical continents and outer rainband region. Such high brightness temperatures are much less frequent in the inner rainband region and especially in the eyewall region. The high brightness temperature end of the distribution is truncated for these regions. In these inner portions of the hurricane, at least some modest 85-GHz ice scattering usually covers a large portion of the total raining area with PCT values below $\approx$265 K. This can be explained by thinking of the hurricane inner core as a ''mixmaster'' (Houze et al. 1992) in which ice particles generated in localized portions of the eyewall are advected across larger areas before falling out as rain. The resulting ice scattering covers a large area, which can complicate TMI-based rainfall retrievals (F. Marks 2000, personal communication). The eyewall region has a broader distribution (a flatter peak on a histogram) of ice scattering signatures than the other hurricane and tropical oceanic regions, similar to the broad distribution of rain rates noted for the eyewall by Marks et al. (1993).

c. Lightning flash densities

Due to the combination of low flash rates and the limited area covered by the eyewall region and inner rainband region, very little lightning was observed in these regions (Table 4). After normalizing the flash counts by sample size for each region (the second column in Table 4; this column is inversely proportional to the spatial flash density), lightning production in the eyewall region is comparable to that in the outer rainband region. Both of these produce about four times as much lightning (per unit area of rainfall) as the inner rainband region and general tropical oceanic sample. The tropical continental sample produces much more lightning than any of the others.

The lack of lightning in the inner rainband region compared to the rest of the hurricane is consistent with the results of Molinari et al. (1999). However, Molinari et al. found flash rate densities to be two to three times greater for the 200–300-km radius region than for the 0–60-km radius region (representing outer rainband regions and eyewall regions, respectively). This difference should be *magnified* when the flash rate densities are normalized by the *raining* area (second column of Table 4), because the fractional coverage by rain decreases with increasing radius. That such a difference is not present in the second column of Table 4 could result from an increased ratio of in-cloud versus cloud-to-ground lightning flashes in the eyewall (this study includes both types whereas Molinari et al. is limited to cloud to ground). It could also result from deficiencies in the sample size and representativeness of either study. This study is limited to very short duration observations of 45 hurricanes around the globe; Molinari et al. were limited to much longer duration observations of only nine hurricanes *near land.*

Because stratiform rain and weak convection compose a large portion of the database but do not contribute greatly to the lightning flash count, additional methods for normalizing the flash counts are presented in Table 4. The volumetric rainfall near the surface (from the version 4 PR algorithm) combines effects from precip-

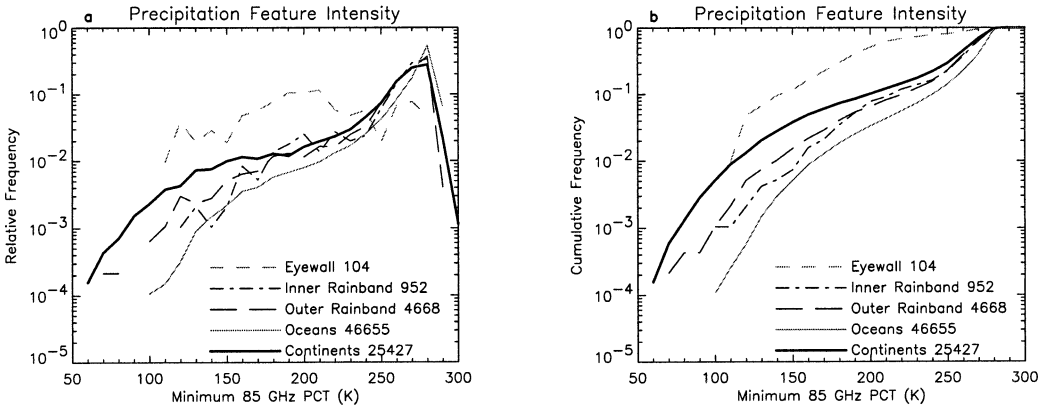

FIG. 7. (a) Probability distribution of precipitation feature minimum 85-GHz PCT (10-K intervals). Sample size is listed for each region. (b) Cumulative density function of precipitation feature minimum 85-GHz PCT.

itation areal coverage and precipitation intensity. The last three columns in Table 4 make use of the criteria used previously to isolate more intense portions of the reflectivity and ice scattering distributions. Compared to the tremendous amount of lightning produced in the tropical continental sample, all of the hurricane and tropical oceanic categories have low flash densities that are roughly similar to each other. However, lightning production is two to four times greater in the outer rainband region than in the general tropical oceanic sample. Given the small sample sizes for the eyewall region and inner rainband region, it is difficult to say if lightning production in these categories is significantly different from that in the general tropical oceanic category.

6. Precipitation feature intensities

The preceding results combine all of the measurements from all of the precipitation features encountered. The following results are based on properties of the individual precipitation features. For each precipitation feature the minimum 85-GHz PCT, minimum 37-GHz PCT, maximum radar reflectivity, and flash count are recorded as indicators of system intensity. Although the focus in this study is on hurricane precipitation features, Nesbitt et al. (2000) compared the tropical oceanic and tropical continental samples in detail using some of these (and related) properties. Besides recording these parameters for each precipitation feature, these parameters are also recorded for each orbit. This latter approach is to account for the fact that several noncontiguous precipitation features may compose what is essentially a single rainband or eyewall.

a. Precipitation feature maximum ice scattering

Small precipitation features dominate the size distributions and also impact the brightness temperature distributions. For all categories except the eyewall region, many precipitation features have high minimum brightness temperatures at 85 and 37 GHz (Figs. 7a, 8a). These brightness temperatures where the distributions peak (around 280 K) are not much less than those due to background emissions from the underlying surface. Like the size distributions (not shown), the distributions of eyewall minimum brightness temperatures are distinctly

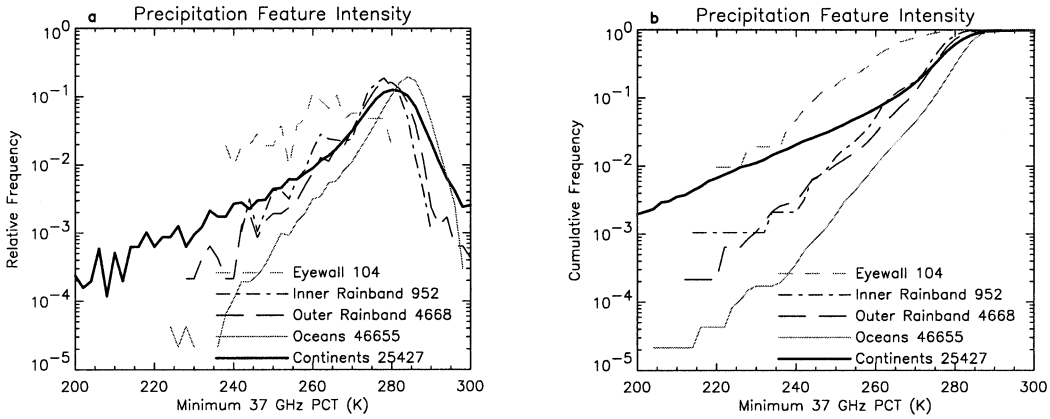

FIG. 8. (a) Probability distribution of precipitation feature minimum 37-GHz PCT (2-K intervals). Sample size is listed for each region. (b) Cumulative density function of precipitation feature minimum 37-GHz PCT.

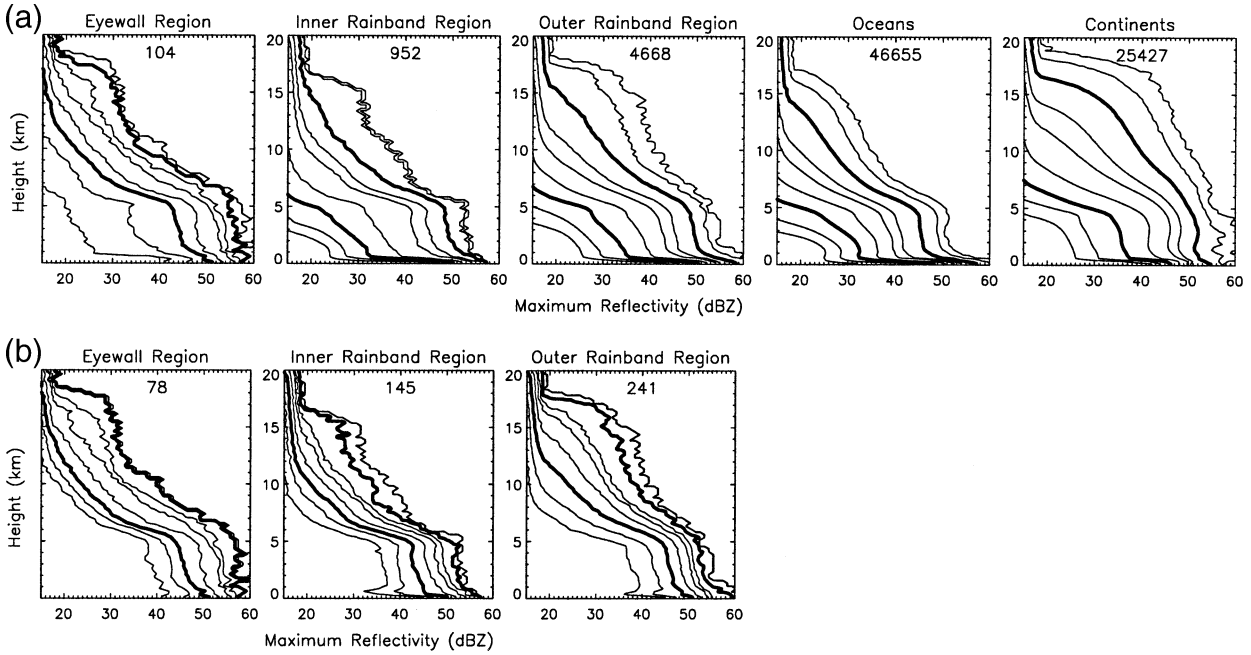

FIG. 9. (a) Cumulative density function of precipitation feature maximum radar reflectivity (1-dBZ intervals) as a function of height. (b) Cumulative density function of precipitation region maximum radar reflectivity as a function of height, combining the individual precipitation features in an individual orbit. Contour levels are 10%, 25%, 50% (bold), 75%, 90%, 95%, 99% (bold), 99.9%, and 99.99%.

different from the other categories. While 80% of the eyewall region precipitation features have minimum 85-GHz PCTs less than 250 K, only 15% of the rainband precipitation features do and 10% of the general tropical oceanic precipitation features meet this 250-K threshold for minimum 85-GHz PCT (Fig. 7b). The most common minimum brightness temperatures for eyewall precipitation features are around 200 K at 85 GHz and 260 K at 37 GHz. Unlike the sharp peaks in the minimum brightness temperature distributions for the other categories, these are very broad peaks for the eyewall region.

In the cumulative frequency distributions at 85 and 37 GHz (Figs. 7b, 8b), the eyewall region precipitation features appear to produce strong ice scattering much more often than precipitation features in any of the other categories. This is almost entirely a result of the relative lack of small precipitation features with high minimum brightness temperatures in the eyewall region. A more informative comparison of the eyewall and rainband regions is possible if the high brightness temperature features (often small features adjacent to larger features with lower brightness temperatures) are removed from the samples. The distributions for the inner rainband region and outer rainband region become more like those for the eyewall region (not shown). This is similar to the normalization applied in section 5b, and the results are similar to those in section 5b. As in section 5b, it becomes apparent that the inner rainband region produces very intense ice scattering features (PCT $<$ 150 K at 85 GHz, $<$250 K at 37 GHz) much less often than do the other regions. An alternate comparison can be made by defining eyewalls and rainbands as sets of precipitation features that are adjacent to each other. This effectively combines the small, high brightness temperature features with larger associated rainbands. Only 3% of such inner rainbands have minimum 85-GHz PCTs below 150 K; about 15% of the eyewalls and outer rainbands reach this level.

b. Precipitation feature maximum reflectivity

Qualitatively, the trends in precipitation feature intensity based on radar reflectivity are similar to those based on ice scattering. That is, all of the samples except for the eyewall region have many precipitation features with low reflectivities and without great vertical development (at least as seen by the PR) (Fig. 9a). When multiple precipitation features from the same orbit are considered to belong to the same entity (as in the preceding paragraph), the weaker features are mostly eliminated (Fig. 9b). Furthermore, it is seen that the inner rainband region rarely produces the kind of reflectivity profile associated with intense convection. In the inner rainband region, the maximum height of the 40-dBZ echo reaches 7 km in less than 1% of the orbits. In the outer rainband region, the 40-dBZ echo reaches 7 km 9% of the time and reaches 8.5 km as often as it reaches 7 km in the inner rainband region. The 40-dBZ echo reaches 7 km 13% of the time in the eyewall region and reaches 10 km as frequently as it reaches 7 km in the inner rainband region. As previously mentioned, the

eyewall temperature anomaly plays a role in the eyewall's enhanced reflectivity at a given height. The warmth of the eyewall is not sufficient, however, to account for the drastic difference between eyewall region and inner rainband region maximum reflectivity. Eyewall convection is aided by the hurricane's secondary circulation, while inner rainband convection tends to be rather weak.

Although the full distributions of reflectivity are given in Fig. 9, they must be used with caution. In the extreme cases, the greatest hurricane reflectivities at high altitudes are from outer rainbands in Fig. 9. This is a misleading result caused by the few intense outer rainbands located over land. These few cases are left in the sample and in the figures because they fit the guidelines outlined in section 2. Any results described in the text have been examined with these cases in mind, to ensure that these cases do not unduly influence the results.

These reflectivity distributions are qualitatively consistent with the profiles presented by Szoke et al. (1986), Black et al. (1996), and others. In these studies, eyewall reflectivities tend to be greater than rainband reflectivities, but this is especially the case above the freezing level. Szoke et al. mean reflectivity profiles are similar above the freezing level for both rainbands and GATE convective cells. The mean eyewall reflectivity profile above the freezing level is more similar to that of the strongest 20% of GATE cells.

7. Summary

In comparison to the intense convective signatures more often found over continents, the radar, ice scattering, and lightning characteristics of hurricane eyewalls, rainbands, and other tropical oceanic features are generally somewhat modest and somewhat similar to each other. As noted in previous studies, the inner rainband region is especially dominated by stratiform rain (Table 1) and rather weak convection. This result is consistent not only with previous radar (Szoke et al. 1986; Black et al. 1996) and lightning (Molinari et al. 1999) studies, but also with the updraft magnitudes presented by Jorgensen et al. (1985) and Black et al. (1996). In the latter two studies, rainbands (generally inner rainbands using the terminology of this study) exhibit weaker updraft magnitudes than do eyewalls. This characteristic of the inner rainband region is also manifested in the radar, ice scattering, and lightning observations of this study. The eyewall region lacks the small features [$O(100\ \text{km}^2)$] and features with minimal to nonexistent ice scattering (PCT values near that of the tropical oceanic background, $\approx$280–290 K) that are abundant in other regions. At the stronger end of the convective spectrum, eyewalls, outer rainbands, and other tropical oceanic systems display similar magnitudes of reflectivity and ice scattering.

For nearly half of the hurricane's raining area, measurable radar echo ($\geq$17 dBZ) does not extend more than 2 km above the freezing level. In the convective regions, the median echo top extends to 8 km in the rainbands (and the rest of the tropical oceans) and to 9 km in the eyewall. Only 2% of the inner rainband region (and also the general tropical oceanic sample) meets the criteria for being identified as ''convective certain''; nearly 4% of the outer rainband region and 9% of the eyewall region meets these criteria. A brightbandlike reflectivity maximum shows up even at the 99th percentile of inner rainband region and general tropical oceanic reflectivities. Even in the highest reflectivity cores of those cases identified as convective certain, the inner rainband region produces a more dramatic decrease of reflectivity above the freezing level (declining from 43 dBZ at 5 km to 35 dBZ at 6 km in Fig. 4) than any of the other regions. Other than the tropical continental sample, the eyewall region has the highest reflectivity in these cores.

High brightness temperatures ($>$275 K) indicative of little or no 85-GHz ice scattering are abundant in the general tropical oceanic, tropical continental, and outer rainband precipitation samples, while much of the inner rainband region and especially the eyewall region often have modest or even moderate ice scattering at 85 GHz (with the PCT depressed to $\approx$200–250 K). In those cases where stronger ice scattering (below $\approx$200 K) is present, a given ice scattering intensity is almost equally likely for the eyewall region, outer rainband region, or general tropical oceanic sample, but least likely in the inner rainband region and most likely over continents.

Normalized by the total precipitation area, lightning flash densities are four times greater in the eyewall region and outer rainband region than in the inner rainband region and the general tropical oceanic sample. However, these flash densities are more than an order of magnitude less than those found over land. The absence of lightning in the inner rainband region can be partly explained by the region's stratiform nature. When normalized by the area occupied by convection, the eyewall region, inner rainband region, and general tropical oceanic sample produce roughly similar amounts of lightning. The small sample size for eyewall and inner rainband lightning limits how detailed a comparison can be made among these three categories. The outer rainband region, on the other hand, produces two to four times more lightning than do nonhurricane tropical oceanic systems. However, the outer rainband region still lags far (more than a factor of 10) behind the tropical continental flash rates.

In section 1, we suggested three possible implications of the known disparity in lightning flash rates between hurricane outer rainbands and the rest of the hurricane. Our analysis of TRMM data suggests that the third of these is true: outer rainbands have higher flash rates despite being comparable in other regards to general tropical oceanic and hurricane convection. Other differences, such as slightly greater reflectivities through the mixed phase region or slightly lower brightness tem-

peratures, are rather subtle. We take these differences as a sign that more supercooled liquid water is present (or that appreciable supercooled water is present more often) in the outer rainbands than elsewhere over the tropical oceans. This is elaborated on in Cecil and Zipser (2002, Part II of the study). In turn, we speculate that updrafts (at least in the lower part of the mixed phase region) tend to be slightly greater in the outer rainbands than elsewhere over the tropical oceans. Updrafts may also be slightly greater in the eyewall region, based on the strength of the reflectivity profiles, but supercooled water is rapidly depleted there by the constant supply of ice particles circulating around the long-lived system. Just as the differences in most observed parameters are subtle, these suggested differences in supercooled liquid water content and updraft magnitude may also be subtle. The sensitivity of lightning to these differences contributes a valuable piece in the puzzle as we try to understand the microphysical makeup of the various storms.

Part II of this study uses the database to address interrelationships between the ice scattering, reflectivity, and lightning characteristics noted here. In particular, the probability of lightning (and how this probability differs from region to region) is examined as a function of 85- and 37-GHz ice scattering and radar reflectivity at different altitudes. The sensitivity of 85- and 37-GHz ice scattering to the height or depth of a reflectivity of a given magnitude is also considered. Reflectivity profiles associated with particular brightness temperatures are compared, as are reflectivity profiles for precipitation features with and without lightning. Future use of this database may include comparisons with precipitation estimates and examination of hurricane intensity or intensity change as this relates to properties of the eyewall and rainbands.

Acknowledgments. Data have been provided by the TRMM Science Data and Information System at GSFC, Greenbelt, Maryland, and the Global Hydrology Resource Center at the Global Hydrology and Climate Center, Huntsville, Alabama. Funding has been provided by NASA Grant NAG-1491. Thanks to Drs. Rick Toracinta, Frank Marks, and Richard Orville, and two anonymous reviewers, for useful comments on this research and manuscript and to Chris West for assistance with much of the computer programming used to build the database.

REFERENCES

Barnes, G. M., E. J. Zipser, D. P. Jorgensen, and F. Marks Jr., 1983: Mesoscale and convective structure of a hurricane rainband. *J. Atmos. Sci.,* **40,** 2125–2137.

Battan, L. J., 1973: *Radar Observation of the Atmosphere.* University of Chicago Press, 234 pp.

Black, M. L., R. W. Burpee, and F. D. Marks Jr., 1996: Vertical motion characteristics of tropical cyclones determined with airborne Doppler radial velocities. *J. Atmos. Sci.,* **53,** 1887–1909.

Black, P. G., R. A. Black, J. Hallett, and W. A. Lyons, 1986: Electrical activity of the hurricane. Preprints, *23d Conf. on Radar Meteorology,* Snowmass, CO, Amer. Meteor. Soc., J277–J280.

Black, R. A. and J. Hallett, 1986: Observations of the distribution of ice in hurricanes. *J. Atmos. Sci.,* **43,** 802–822.

——, and ——, 1999: Electrification of the hurricane. *J. Atmos. Sci.,* **56,** 2004–2028.

Boccippio, D. J., S. J. Goodman, and S. Heckman, 2000: Regional differences in tropical lightning distributions. *J. Appl. Meteor.,* **39,** 2231–2248.

Cecil, D. J. and E. J. Zipser, 1999: Relationships between tropical cyclone intensity and satellite-based indicators of inner core convection: 85-GHz ice-scattering signature and lightning. *Mon. Wea. Rev.,* **127,** 103–123.

——, and ——, 2002: Reflectivity, ice scattering, and lightning characteristics of hurricane eyewalls and rainbands. Part II: Intercomparison of observations. *Mon. Wea. Rev.,* **130,** 785–801.

Christian, H. J., and Coauthors, 1999: The Lightning Imaging Sensor. *Proc. 11th Int. Conf. on Atmospheric Electricity,* Guntersville, AL, International Commission on Atmos. Electricity, 746–749. [Available from NASA Center for AeroSpace Information, 800 Elkridge Landing Rd, Linthicum Heights, MD 21090-2934.]

Houze, R. A., Jr., F. D. Marks Jr., and R. A. Black, 1992: Dual-aircraft investigation of the inner core of Hurricane Norbert. Part II: Mesoscale distribution of ice particles. *J. Atmos. Sci.,* **49,** 943–962.

Igau, R. C., M. A. LeMone, and D. Wei, 1999: Updraft and downdraft cores in TOGA COARE: Why so many buoyant downdraft cores? *J. Atmos. Sci.,* **56,** 2232–2245.

Iguchi, T., T. Kozu, R. Meneghini, J. Awaka, and K. Okamoto, 2000: Rain-profiling algorithm for the TRMM precipitation radar. *J. Appl. Meteor.,* **39,** 2038–2052.

Illingworth, A. J., 1985: Charge separation in thunderstorms: Small scale processes. *J. Geophys. Res.,* **90,** 6026–6032.

Jayaratne, E. R., C. P. R. Saunders, and J. Hallett, 1983: Laboratory studies of the charging of soft-hail during ice crystal interactions. *Quart J. Roy. Meteor. Soc.,* **109,** 609–630.

Jorgensen, D. P., 1984: Mesoscale and convective scale characteristics of mature hurricanes. Part I: General observations by research aircraft. *J. Atmos. Sci.,* **41,** 1268–1285.

——, E. J. Zipser, and M. A. LeMone, 1985: Vertical motions in intense hurricanes. *J. Atmos. Sci.,* **42,** 839–856.

——, and M. A. LeMone, 1989: Vertical velocity characteristic of oceanic convection. *J. Atmos. Sci.,* **46,** 621–640.

Kummerow, C., W. Barnes, T. Kozu, J. Shiue, and J. Simpson, 1998: The Tropical Rainfall Measuring Mission (TRMM) sensor package. *J. Atmos. Oceanic Technol.,* **15,** 809–817.

——, and Coauthors, 2000: The status of the Tropical Rainfall Measuring Mission (TRMM) after two years in orbit. *J. Appl. Meteor.,* **39,** 1965–1982.

LeMone, M. A., and E. J. Zipser, 1980: Cumulonimbus vertical velocity events in GATE. Part I: Diameter intensity and mass flux. *J. Atmos. Sci.,* **37,** 2444–2457.

Ligda, M. G. H., 1955: Analysis of motion of small precipitation areas and bands in the hurricane August 23–28, 1949. Department of Meteorology Tech. Note 3, Massachusetts Institute of Technology, 36 pp.

Lucas, C., E. J. Zipser, and M. A. LeMone, 1994: Vertical velocity in oceanic convection off tropical Australia. *J. Atmos. Sci.,* **51,** 3183–3193.

Lyons, W. A., and C. S. Keen, 1994: Observations of lightning in convective supercells within tropical storms and hurricanes. *Mon. Wea. Rev.,* **122,** 1897–1916.

Marks, F. D., Jr., and R. A. Houze Jr., 1987: Inner core structure of Hurricane Alicia from airborne Doppler radar observations. *J. Atmos. Sci.,* **44,** 1296–1317.

——, D. Atlas, and P. T. Willis, 1993: Probability-matched reflectivity–rainfall relations for a hurricane from aircraft observations. *J. Appl. Meteor.,* **32,** 1134–1141.

Mohr, K. I., and E. J. Zipser, 1996: Defining mesoscale convective

systems by their 85-GHz ice-scattering signatures. *Bull. Amer. Meteor. Soc.*, **77,** 1179–1189.
——, J. S. Famiglietti, and E. J. Zipser, 1999: The contribution to tropical rainfall with respect to convective system type, size, and intensity estimated from the 85-GHz ice-scattering signature. *J. Appl. Meteor.*, **38,** 596–606.
Molinari, J., P. Moore, and V. Idone, 1999: Convective structure of hurricanes as revealed by lightning locations. *Mon. Wea. Rev.*, **127,** 520–534.
Nesbitt, S. W., E. J. Zipser, and D. J. Cecil, 2000: A census of precipitation features in the Tropics using TRMM: Radar, ice scattering, and lightning observations. *J. Climate*, **13,** 4087–4106.
Petersen, W. A., and S. A. Rutledge, 2001: Regional variability in tropical convection: Observations from TRMM. *J. Climate*, **14,** 3566–3586.
Reynolds, S. E., M. Brook, and M. F. Gourley, 1957: Thunderstorm charge separation. *J. Meteor.*, **14,** 426–436.
Rodgers, E. B., R. F. Adler, and H. F. Pierce, 2000: Contribution of tropical cyclones to the North Pacific climatological rainfall as observed from satellites. *J. Appl. Meteor.*, **39,** 1658–1678.
Samsury, C. E., and R. E. Orville, 1994: Cloud-to-ground lightning in tropical cyclones: A study of Hurricanes Hugo (1989) and Jerry (1989). *Mon. Wea. Rev.*, **122,** 1887–1896.
——, and E. J. Zipser, 1995: Secondary wind maxima in hurricanes: Airflow and relationship to rainbands. *Mon. Wea. Rev.*, **123,** 3502–3517.
Saunders, C. P. R., and S. L. Peck, 1998: Laboratory studies of the influence of the rime accretion rate on charge transfer during crystal/graupel collisions. *J. Geophys. Res.*, **103,** 13 949–13 956.
——, W. D. Keith, and R. P. Mitzeva, 1991: The influence of liquid water on thunderstorm charging. *J. Geophys. Res.*, **96,** 11 007–11 017.
Senn, H. V., and H. W. Hiser, 1959: On the origin of hurricane spiral rainbands. *J. Meteor.*, **16,** 419–426.
Spencer, R. W., 1986: A satellite passive 37-GHz scattering-based method for measuring oceanic rain rates. *J. Climate Appl. Meteor.*, **25,** 754–766.
——, H. M. Goodman, and R. E. Hood, 1989: Precipitation retrieval over land and ocean with the SSM/I: Identification and characteristics of the scattering signal. *J. Atmos. Oceanic Technol.*, **6,** 254–273.
Szoke, E. J., E. J. Zipser, and D. P. Jorgensen, 1986: A radar study of convective cells in mesoscale convective systems in GATE. Part I: Vertical profile statistics and comparisons with hurricane cells. *J. Atmos. Sci.*, **43,** 182–197.
Takahashi, T., 1978: Riming electrification as a charge generation mechanism in thunderstorms. *J. Atmos. Sci.*, **35,** 1536–1548.
Tibbets, R. T., and T. N. Krishnamurti, 2000: An intercomparison of hurricane forecasts using SSM/I and TRMM rain rate algorithm(s). *Meteor. Atmos. Phys.*, **74,** 37–49.
Toracinta, E. R., D. J. Cecil, E. J. Zipser, and S. W. Nesbitt, 2002: Radar, passive microwave, and lightning characteristics of precipitating systems in the Tropics. *Mon. Wea. Rev.*, **130,** 802–824.
Wexler, H., 1947: Structure of hurricanes as determined by radar. *Ann. N. Y. Acad. Sci.*, **48,** 821–844.
Wilheit, T. T., 1986: Some comments on passive microwave measurement of rain. *Bull. Amer. Meteor. Soc.*, **67,** 1226–1232.
Willoughby, H. E., 1990: Temporal changes of the primary circulation in tropical cyclones. *J. Atmos. Sci.*, **47,** 242–264.
——, F. D. Marks Jr., and R. J. Feinberg, 1984: Stationary and moving convective bands in hurricanes. *J. Atmos. Sci.*, **41,** 3189–3211.
Wu, R., and J. A. Weinman, 1984: Microwave radiances from precipitating clouds containing aspherical ice, combined phase, and liquid hydrometeors. *J. Geophys. Res.*, **89,** 7170–7178.
Zipser, E. J., and K. R. Lutz, 1994: The vertical profile of radar reflectivity of convective cells: A strong indicator of storm intensity and lightning probability? *Mon. Wea. Rev.*, **122,** 1751–7159.